Incorporating Wave Spectrum Information in Real-time Free-surface Elevation Forecasting: Real-sea Experiments

Alexis Mérigaud [*] James Herterich [**,***] Jason Flanagan [****]
John Ringwood [*] Frederic Dias [**,***]

[*] Centre for Ocean Energy Research, Maynooth University, Maynooth, co. Kildare, Ireland
[**] UCD School of Mathematics and Statistics, University College Dublin, MaREI Centre, Dublin, Ireland
[***] UCD Earth Institute, University College Dublin, Dublin, Ireland
[****] ICHEC, NUI Galway, Galway City, Ireland

Abstract: Real-time prediction of free-surface elevation is necessary for a variety of applications. Assuming a Gaussian wave field, the wave spectrum can be used to calculate the statistically-optimal predictor, for a given prediction configuration (i.e. for a given combination of measurement instants and spatial locations, relative to the instants and locations where and when the wave is predicted). More specifically, the optimal predictor is linear, and its coefficients need only be updated as the wave condition evolves. This spectrum-based prediction (SBP) approach encompasses, in a unified theoretical framework, both "time-series" and "spatially-distributed" prediction configurations. In this paper, the validity of the SBP theoretical framework is tested against real-sea wave data, which originate from a measurement campaign using an Acoustic Doppler Current Profiler (ADCP), and consist of free-surface elevation time series, at the corners and centre of a 25m-by-25m square. The directional wave spectra, corresponding to the sea states where the time series are provided, have also been calculated. The empirical SBP accuracy, obtained by applying the SBP in the real-sea time series, is assessed in various sea conditions and prediction configurations, and compared with the theoretical SBP accuracy, evaluated based on the wave spectra. Although the ADCP measurement layout is clearly not ideal for the purpose of wave forecasting, empirical results are physically and statistically consistent, and show good agreement with theoretical results, thus supporting the relevance of the SBP framework.

1. INTRODUCTION

Real-time prediction of sea surface elevation has received significant interest in the past 20 years, see Abusedra and Belmont (2011). Applications include the detection of quiescent periods for safe marine operations, as reviewed by Giron-Sierra and Esteban (2010), and real-time optimal control of wave energy converters (WECs) to improve power capture, as investigated by Fusco and Ringwood (2010).

Two main approaches are generally considered for short-term wave forecasting:

- methods based on spatial prediction of wave elevation, through physical or stochastic propagation models, requiring observations in the vicinity of the point of interest, see e.g. Belmont et al. (2014); Abusedra and Belmont (2011); Naaijen and Blondel-Couprie (2012);
- methods using only past measurements at the point of interest, thus treating the wave elevation as a time series, as in Fusco and Ringwood (2010).

The two categories of methods are hereafter termed "spatially-distributed" and "time-series" techniques, respectively.

A recent study by Mérigaud and Ringwood (2018) considers the general problem of the statistically-optimal predictor for a given prediction configuration, i.e. for a given, discrete set of *observation points* (at different instants in time and possibly different spatial locations) used to predict the wave elevation at a given, discrete set of *prediction points*. Assuming stationary Gaussian waves, and for a given prediction configuration, Mérigaud and Ringwood (2018) show that the optimal predictor is linear, and that its coefficients can be calculated from the wave spectrum, assuming that the latter is known.

Several characteristics make the method (hereafter termed the spectrum-based predictor, or SBP) theoretically attractive. Firstly, under the assumption of a stationary, Gaussian wave field, and assuming perfect knowledge of the wave spectrum, the SBP is statistically optimal (in a mean-square error sense) for a given prediction configuration. Secondly, the SBP handles in a unified framework

both spatially-distributed and time-series approaches. Finally, instead of requiring identification of prediction coefficients based on a long dataset, the SBP directly makes use of wave spectrum information. However, the practical applicability of the SBP remains to be demonstrated, since Mérigaud and Ringwood (2018) only show theoretical results - using idealised spectral formulations as examples.

A scientific wave measurement campaign was run in 2017 by University College Dublin, deploying state-of-the-art ADCP technology, off Inis Meáin, Co. Galway, off the West coast of Ireland, with the aim of recording extreme wave conditions, similarly to the 2015 campaign reported by Flanagan et al. (2016). The bed-mounted, Sentinel V ADCP [1] has 5 acoustic sensors, forming 5 beams along which echo intensity and particle velocity are recorded. ADCP measurements have been used to reconstruct wave elevation time series at the five points, formed by the beam intersections with the ocean surface. Besides, half-hourly directional wave spectra have been estimated from the ADCP measurements.

The ADCP layout is not ideal for the purpose of wave prediction, for two main reasons:

- As calculated in several studies using different methods (Abusedra and Belmont (2011); Mérigaud and Ringwood (2018); Naaijen et al. (2014)), a long forecast horizon necessitates that measurements are taken far up-wave with respect to the point of interest (typically, several hundred meters for a 1-min time horizon, the exact ratio depending on the maximum group velocity present in the wave spectrum). In comparison, the maximum distance between two measurement points of the ADCP is 40m;
- The examples provided by Mérigaud and Ringwood (2018), for 3D wave fields, seem to indicate that, even with sharply concentrated spectra, directional spreading affects significantly the quality of the forecasts obtained using spatially-distributed measurements. More specifically, accurate forecasts would require a large number of up-wave measurement points (typically more than 10) to capture the wave directionality. In contrast, the ADCP layout consists of five measurement points only.

Nevertheless, the data obtained from the ADCP measurement campaign contain good-quality real-sea wave time series, along with the directional wave spectra for the sea-states where those measurements were recorded. Therefore, although not ideal, the dataset resulting from the campaign provided a valuable opportunity for the authors to investigate the SBP practical applicability. The objective of this study is not to promote the use of ADCP as a wave forecasting set-up, but merely to check the validity of the theoretical framework proposed by Mérigaud and Ringwood (2018), against an appropriate real-sea dataset.

The remainder of this paper is organised as follows: the SBP approach is detailed in Section 2, and the ADCP measurement layout and the resulting wave dataset are described in Section 3. Sample experimental results are shown in Section 4. Finally, conclusions are drawn in Section 5.

---

[1] http://www.teledynemarine.com/rdi/

2. SPECTRUM-BASED PREDICTION

2.1 Wave spectrum and space-time correlation function

Assume a Gaussian, stationary, homogeneous and ergodic random wave field - which, see for example Ochi (2005), excludes severe storms and shallow water conditions. The waves are characterised by a directional spectral density function $S(\omega, \theta)$, where ω denotes the frequency and θ denotes an angle relative to a reference direction.

For waves with a given frequency ω, the wave dispersion equation defines how ω and the wave number k are related to each other. In the general case, for intermediate water depths, the dispersion relation is written as:

$$\omega^2 = gk \tanh(hk) \qquad (1)$$

where g is the acceleration due to gravity and h the water depth. In practice, Eq. (1) defines an implicit function $k(\omega)$, which can be numerically evaluated for any arbitrary ω.

Consider the random experiment of measuring the wave elevation, η, at two different times (t_1 and t_2) and two different locations ($\mathbf{x}_1$ and $\mathbf{x}_2$). By definition of a Gaussian field, the two measurements are jointly Gaussian. Furthermore, because of the stationarity and homogeneity assumption, the covariance of the two measurements, $\mathbb{E}[\eta(\mathbf{x}_1, t_1)\eta(\mathbf{x}_2, t_2)]$, only depends on the *relative location* and *relative instant* of the two measurements. More specifically, denoting $\mathbf{r} = \mathbf{x}_2 - \mathbf{x}_1$ as relative spatial coordinates, and $\tau = t_2 - t_1$ as the relative measurement instant, the space-time covariance function can be derived from the directional spectrum as follows - see de Boer (1969):

$$R_{\eta\eta}(\mathbf{r}, \tau) = \int_{-\pi}^{\pi} d\theta \int_{0}^{\infty} d\omega S(\omega, \theta) \cos[k(\omega)\mathbf{r}.\mathbf{u}_\theta - \omega\tau] \qquad (2)$$

where $\mathbf{u}_\theta$ is the unit vector with direction θ. (2) is the 3-dimensional equivalent of the well-known Wiener-Khinchin theorem, see e.g. Ochi (2005).

In summary, the covariance of any given pair of measurements, taken at two different instants and locations, can be derived from the wave spectrum using (2).

2.2 Statistically-optimal predictor

Consider:

- a finite, discrete set of M wave *observations*, taken at various points in space and time, together forming a multivariate, Gaussian random vector, denoted $\mathbf{p}$;
- a finite, discrete set of N wave *unknown values*, taken at various points in space and time, together forming a multivariate, Gaussian random vector, denoted $\mathbf{q}$.

The prediction problem consists of calculating the best estimate for $\mathbf{q}$, using observations $\mathbf{p}$. Define

$$\mathbf{v} = \begin{pmatrix} \mathbf{p} \\ \mathbf{q} \end{pmatrix} \qquad (3)$$

and $(\mathbf{r}_i, t_i)$ the space-time coordinate of the i-th random component of $\mathbf{v}$. $\mathbf{v}$ is a multivariate Gaussian random vector. Its mean is $0_{\mathbb{R}^{M+N}}$ and its covariance matrix, noted $\mathbf{\Sigma_{vv}}$, can be derived from the correlation values between

any pair of points in time and space, i.e. $\Sigma_{\mathbf{vv}i,j} = R_{\eta\eta}(\mathbf{r}_j - \mathbf{r}_i, t_j - t_i)$ calculated using (2).

$\Sigma_{\mathbf{vv}}$ can be written as:

$$\Sigma_{\mathbf{vv}} = \begin{pmatrix} \Sigma_{\mathbf{qq}} & \Sigma_{\mathbf{qp}} \\ \Sigma_{\mathbf{pq}} & \Sigma_{\mathbf{pp}} \end{pmatrix} \qquad (4)$$

where $\Sigma_{\mathbf{qp}} = \Sigma_{\mathbf{pq}}^{\mathrm{T}}$. The conditional distribution of $\mathbf{q}|\mathbf{p}$ is multivariate Gaussian (see for example Eaton (2007)) and, using $\mu_{\mathbf{p}} = \mu_{\mathbf{q}} = 0$, its mean is:

$$\mu_{\mathbf{q}|\mathbf{p}} = \Sigma_{\mathbf{qp}} \Sigma_{\mathbf{pp}}^{-1} \mathbf{p} \qquad (5)$$

and its variance is:

$$\Sigma_{\mathbf{q}|\mathbf{p}} = \Sigma_{\mathbf{qq}} - \Sigma_{\mathbf{qp}} \Sigma_{\mathbf{pp}}^{-1} \Sigma_{\mathbf{pq}} \qquad (6)$$

The best predictor of $\mathbf{q}$, in a least mean-square sense, is given as $\tilde{\mathbf{q}} = \mu_{\mathbf{q}|\mathbf{p}}$.

For a stationary, homogeneous wave field, the covariance of observation and prediction points only depends on their *relative position* in time and space; in other words, $\Sigma_{\mathbf{vv}i,j} = R_{\eta\eta}(\mathbf{r}_j - \mathbf{r}_i, t_j - t_i)$. Hence, the prediction matrix, $\mathbf{Q} := \Sigma_{\mathbf{qp}} \Sigma_{\mathbf{pp}}^{-1}$, which maps M observed values to N predicted values, also depends solely on the *relative position* of observation and prediction points.

Define a *measurement configuration* as the relative spatial and temporal coordinates of the components of $\mathbf{p}$ and $\mathbf{q}$. If the measurement configuration is constant, the prediction matrix, $\mathbf{Q}$, needs only be computed once for a given sea condition, and thus needs only be updated as the wave spectrum evolves significantly, for example every 30 minutes. Therefore, the only operation to be carried out in real time is the matrix multiplication $\tilde{\mathbf{q}} = \mathbf{Q}\mathbf{p}$.

For example, consider an experiment where η is measured at a location $\mathbf{x}_{\mathrm{obs}}$ to predict η at another location $\mathbf{x}_{\mathrm{pred}}$. The sampling time is Δt and the prediction is carried out every Δt seconds. At the kth instance of the prediction, at $k\Delta t$, the observations are the latest M measured values of η at $\mathbf{x}_{\mathrm{obs}}$, i.e. $\mathbf{p}_i = \eta(\mathbf{x}_{\mathrm{obs}}, i\Delta t)$ for $i = k - M + 1, ..., k$. The predicted values are the wave elevation at $\mathbf{x}_{\mathrm{pred}}$ over, say, the next N sampling instants, i.e. $\mathbf{q}_j = \eta(\mathbf{x}_{\mathrm{pred}}, j\Delta t)$ for $j = k+1, ..., k+N$. In such an experiment, the relative spatial and temporal coordinates corresponding to the components of $\mathbf{p}$ and $\mathbf{q}$ are the same at each instance k of the prediction, and thus the prediction matrix $\mathbf{Q}$ needs only be calculated once for a given sea state.

The theoretical mean-square prediction error $\epsilon^2 \in \mathbb{R}^N$, which characterises the error for each component of the predicted vector $\tilde{\mathbf{q}}$, is given by the diagonal terms of $\Sigma_{\mathbf{q}|\mathbf{p}}$. For a given measurement configuration, any other forecasting method is sub-optimal with respect to the law derived in (5).

2.3 Accounting for measurement noise

Although theoretically attractive, deriving the prediction matrix $\mathbf{Q}$ from the wave spectrum requires some care when exerted in practice. In particular, measurement noise must be taken into account. For example, assuming that the measurement errors are stationary white noise (i.e. uncorrelated in time and space), with variance σ^2, then the diagonal terms of $\Sigma_{\mathbf{pp}}$ should be modified as $\Sigma_{\mathbf{pp}i,i} = R_{\eta\eta}(0,0) + \sigma^2$, instead of $R_{\eta\eta}(0,0)$, prior to calculating $\mathbf{Q}$.

As will be exemplified in Section 4, failing to do so can result in the predictor being exceedingly sensitive to the presence of noise in actual measurements.

3. REAL WAVE DATASET

A state-of-the-art Sentinel V ADCP was deployed at a site off the West coast of Ireland [2], throughout the winter and spring 2017, in order to gather accurate wave measurements in extreme conditions. The Sentinel V comprises 5 acoustic sensors (1 vertical beam and 4 slant beams, forming a 25° angle with the vertical beam), and records echo intensity and velocity values along each beam. A quality control procedure, described in Flanagan et al. (2016), was implemented in order to clean the data, and wave elevation time series were computed, at the locations formed by the intersection of each beam with the free-surface. The free-surface heights are corrected for the pitch, roll, and heading of the ADCP device, and converted from instrument coordinates to geographical coordinates using standard transformations [3]. The time series are organised in half-hourly data-sets, with a 0.5s sampling time, and they are corrected from the effect of tidal changes. Flanagan et al. (2016) provide additional detail about the ADCP set-up.

The corresponding half-hourly directional spectral density functions (SDF) were calculated, using the Bayesian directional spectrum estimation method (BDM) proposed by Hashimoto (1997), and implemented in the Matlab [4] DIWASP [5] toolbox. The DIWASP inputs are the half-hourly surface-height measurements from the four slant beams and their positions. For this study, SDFs have a 0.5° angular resolution, and a 0.005Hz frequency resolution, ranging from 0.005 to 1Hz (the latter being the Nyquist frequency for the 0.5s sampling interval). The SDF is denoted $S(f, \theta)$. For this study, the spectra are further smoothed through a 1h30 moving average, i.e. by averaging $S(f, \theta)$ at the kth half-hour with $S(f, \theta)$ at the $k - 1^{\mathrm{th}}$ and $k + 1^{\mathrm{th}}$ half-hours. Thus, the spectral estimates used for SBP are less dependent on short-term randomness.

Two particular days of data are considered for the purpose of this study, and contrasted in Figs 1 and 2: one with relatively low sea states (5th Jan 2017 starting 0:00am; average significant wave height $H_{m_0} = 1.73$m), and one with significantly more energetic seas (9th Jan 2017 starting 11:03am; $H_{m_0} = 4.86$m on average).

The positions of the points formed by the intersection of each beam with the free-surface are denoted VB (for the vertical beam) and SB1, ... SB4 (for the slant beams). In Fig. 1, the average positions of SBs 1-4 relative to VB are indicated, along with the average directional distribution of the wave spectral energy, for the two days considered. A 0° angle indicates waves propagating from the North; a 270° angle indicates waves propagating from the West (which is the most common situation off the West Irish coast). Waves on the 5th Jan mainly come from a South-West direction, facing the SB3-SB2 side of the square, al-

[2] West of the Aran islands; the ADCP frame has coordinates (53°4.0285 N', −009°37.596 W')

[3] ADCP Coordinate Transformation: Formulas and Calculations. Teledyne RD Instruments (2010)

[4] www.mathworks.co.uk

[5] DIrectional WAve SPectra, see www.metocean.com

though some smaller energy content appears coming from other directions. In contrast, on the 9th Jan, the waves are sharply focused, coming from a westerly direction.

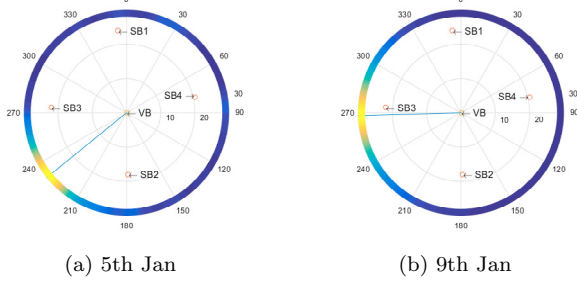(a) 5th Jan   (b) 9th Jan

Fig. 1. ADCP measurement layout and average wave directional spreading, for the two datasets.

The two datasets are further contrasted by examining Fig. 2, where the spectral frequency content (i.e. integrated over all directions) are compared for the two days. Wave energy on the 9th Jan is sharply concentrated around low frequencies ($T_p \approx 14s$), while the 5th Jan exhibits a higher-frequency content, and bimodal characteristics. The latter case is unfavourable from the point of view of wave forecasting, as documented by Mérigaud and Ringwood (2018).

4. EXPERIMENTAL RESULTS

4.1 Prediction configurations

Spatial prediction configurations are abbreviated in the form {measurement locations} → {prediction location}. For example, {SB1, SB2, SB3, VB} → {SB4} indicates that η at SB4 is predicted using the latest measurements at the four other beams.

Define T_l as the time duration over which latest observed values are used for the prediction. Assume for example {SB1} → {VB}. At instant $t_k = k\Delta t$, the prediction for $\eta(\mathbf{x}_{VB}, t_{k+i})$ is calculated, using $\mathbf{p} = [\eta(\mathbf{x}_{SB1}, t_{k-M}), ...\eta(\mathbf{x}_{SB1}, t_k)]^T$, where $M\Delta t = T_l$. In all prediction configurations presented throughout the rest of this paper, $T_l = 60s$ (therefore $M = 60/\Delta t = 120$), since a short preliminary study suggested no benefit in further increasing T_l.
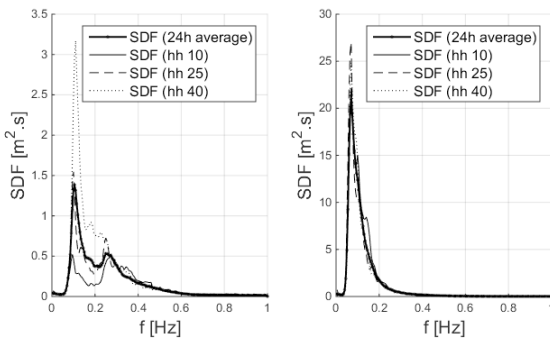

Fig. 2. Non-directional spectra: 24-h average, and 10th, 25th and 40th half-hourly spectra, on the 5th Jan (left) and 9th Jan (right). For readability the two plots have different scales.

4.2 Performance metrics

Denoting $\epsilon^2(i\Delta t)$ the mean-square prediction error for the time horizon $i\Delta t$, the SBP accuracy is assessed for each i using the goodness of fit (GoF) as a performance metrics:

$$G(i\Delta t) = 1 - \sqrt{\frac{\epsilon^2(i\Delta t)}{\mathbb{E}[\eta^2]}} \qquad (7)$$

where a GoF of 1 indicates perfect prediction [6].

For a given half-hourly data-set, and for a given prediction configuration, the prediction matrix $\mathbf{Q}$ and error matrix $\boldsymbol{\Sigma}_{\mathbf{q|p}}$ are computed using (5) and (6), derived from the half-hourly spectrum as explained in Section 2.1. The *theoretical* GoF, $G_{th}(i\Delta t)$, predicted by the SBP theory, is obtained using (7), where $\epsilon^2(i\Delta t)$ is given by the diagonal terms of $\boldsymbol{\Sigma}_{\mathbf{q|p}}$ and $\mathbb{E}[\eta^2] = m_0$ (obtained as the area under $S(\omega, \theta)$). G_{th} thus only depends on the wave spectrum.

The *empirical* GoF is estimated from the actual mean-square error, calculated by applying SBP in the actual time series and comparing predicted with actual values. More specifically, denote, $\forall n$, $\eta_n = \eta(n\Delta t)$ at the beam where η is predicted, and $\tilde{\eta}_{k+i|k}$ the predicted value for η_{k+i}, as predicted at instant t_k. Then, for each time horizon $i\Delta t$, $G_{emp}(i\Delta t)$ is estimated as:

$$G_{emp}(i\Delta t) = 1 - \sqrt{\frac{\frac{1}{N_s - N_h - M + 1}\sum_{k=M}^{N_s - N_h}(\tilde{\eta}_{k+i|k} - \eta_{k+i})^2}{\frac{1}{N_s}\sum_{k=M}^{N_s - N_h}\eta_k^2}}$$

$$(8)$$

where $N_s = 1800/\Delta t = 3600$ is the number of samples in a half-hourly data-set, $M\Delta t = T_l = 60s$ as explained in Section 4.1, and $N_h\Delta t = T_h$ is the maximum time horizon considered (20s for the results shown in this study).

4.3 Calibration of the measurement noise model

The variance m_0 of the wave signal, recorded at the SBs, is slightly larger than that recorded at the VB, by approximately $0.1m^2$, due to noisier backscattering at the SBs. As explained in Section 2.3, and assuming white noise errors, this can be taken into account by adding the appropriate noise variance, σ^2, to the diagonal terms of $\boldsymbol{\Sigma}_{\mathbf{pp}}$ corresponding to the SBs, prior to computing the prediction matrix $\mathbf{Q}$.

A short calibration study was carried out, to determine the appropriate noise level σ^2 that should be modelled in $\boldsymbol{\Sigma}_{\mathbf{pp}}$. Using {SB1,SB2,SB3,SB4}→{VB} as a configuration, G_{emp}, obtained assuming various levels of white noise, is shown in Fig. 3, for the 40th half-hourly dataset of the 9th Jan. G_{th}, computed from the corresponding half-hourly spectrum (without assuming any white noise) is also plotted for comparison. It can be seen that, if σ^2 is assumed zero or too small when computing $\mathbf{Q}$, the SBP performs poorly, yielding sometimes negative values for G_{emp}. When the noise level is appropriately quantified, ($\sigma^2 \approx 0.1m^2$), G_{emp} closely matches G_{th}. Finally, over-estimating σ^2 does not significantly affect the predictor

---

[6] Note that G is a less flattering metrics than the correlation C, used by Belmont et al. (2014) and other authors: using orthogonality of predictions and errors under optimal forecast, it can be shown that $C = \sqrt{G(2 - G)}$, so that $G = 50\%$ corresponds to $C = 87\%$.
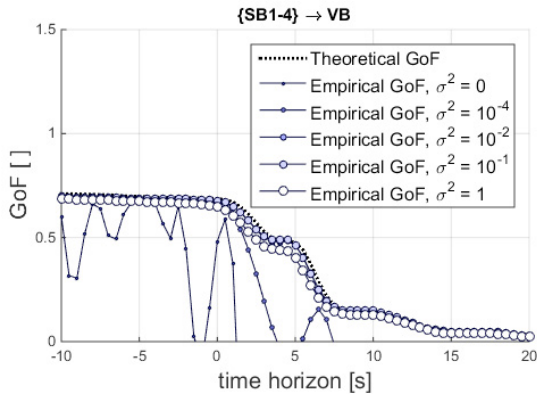
Fig. 3. Calibration of the measurement noise model. Configuration {SB1,SB2,SB3,SB4}→{VB}. 40th half-hour of the 9th Jan dataset.

performance. In the remainder of this study, σ^2 is modelled at $\sigma^2 = 0.2 m^2$ for the computation of $\mathbf{Q}$.

In Fig. 3, note that negative time horizons correspond to *reconstructions*, as opposed to proper *forecasts*.

4.4 Sample results

For the sample numerical results presented in this paper, predictions at VB (the central beam) and SB4 (which is "down-wave" with respect to all other beams) are carried out, in each half-hourly dataset of both 5th and 9th Jan, using three prediction configurations:

- "time-series" (TSC): {beam of interest} → {beam of interest};
- "spatially distributed" (SDC): {*all other* beams} → {beam of interest};
- "mixed" (MC): {*all* beams} → {beam of interest}.

Empirical results, i.e. G_{emp}, are shown in Fig. 4 for three different half-hours of each day, along with G_{emp} averaged over the 48 half-hours of each day. In addition, G_{th} corresponding to the MC is shown for each case, assuming no measurement noise.

The first striking feature of the results is the relatively poor predictor performance, with both theoretical and empirical GoFs fading out to zero after as little as 20s, at best. This is because the five observation points are too close to each other to provide information sufficiently in advance, as mentioned in the introduction. In the MC, G_{emp} and G_{th} show reasonable agreement, although the latter, obtained assuming no measurement noise, is always slightly better. The discrepancies are larger when η is predicted at VB, than when η is predicted at SB4. Overall, G_{th} provides a reliable upper bound to the accuracy which can be expected, in a given prediction configuration and wave spectrum.

Compared to the TSC, the SDC makes use of up-wave information - and thus has a larger forecasting horizon. This is particularly the case at SB4, due to its down-wave location with respect to the other beams (while, in contrast, at VB the forecasting horizon is barely improved by measurements at other beams). Compared to the SDC, TSC makes use of past wave observations at the beam of interest - and thus has a GoF of 1 for negative time
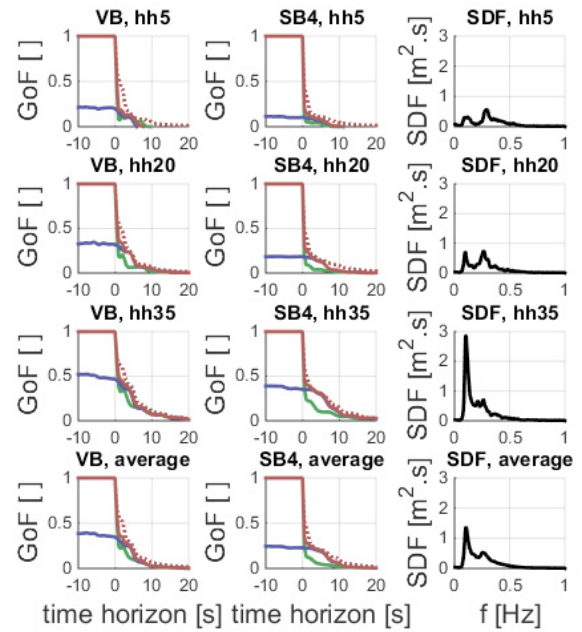
(a) 5th Jan.
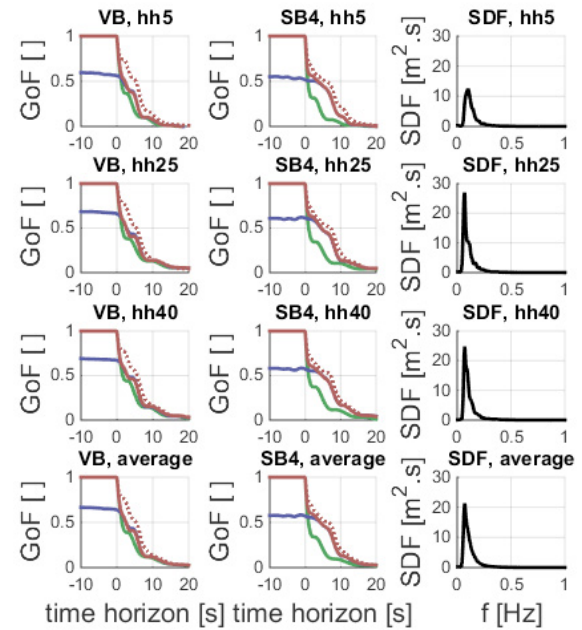
(b) 9th Jan.

Fig. 4. Empirical and theoretical GoFs, in various sea states and prediction configurations. For both days, the ith half-hourly dataset is denoted "hh$i$".

horizons. The MC combines the observations of both TSC and SDC, and thus performs better for all time horizons.

With the SDC, waves can be, to some extent, predicted at the beam of interest, using measurements at other beams. In particular, η at VB can be better reconstructed (i.e. predicted for negative time horizons) than that at SB4,

because of the central location of VB. In contrast, given the "down-wave" location of SB4, the forecasting horizon is better at SB4 than at VB, but the reconstruction is worse. The fact that the reconstruction GoF is not 1 can be interpreted as a result of the wave directional spreading, which prevents all wave information from being captured through only four measurement points.

Comparing the variety of sea states across the two datasets, it can be appreciated how the wave spectrum characteristics affect the prediction accuracy. Sea states with a broad frequency content (e.g. hh5, hh20 of the 5th Jan dataset) result in extremely poor accuracy for all prediction configurations, while more sharply concentrated sea states (e.g. hh35 of the 5th Jan dataset, all sea states of the 9th Jan dataset) are significantly more favourable.

(a) Meas. layout (3 rows at resp. 60, 120 and 180m up-wave). η is predicted at the centre of the diagram.
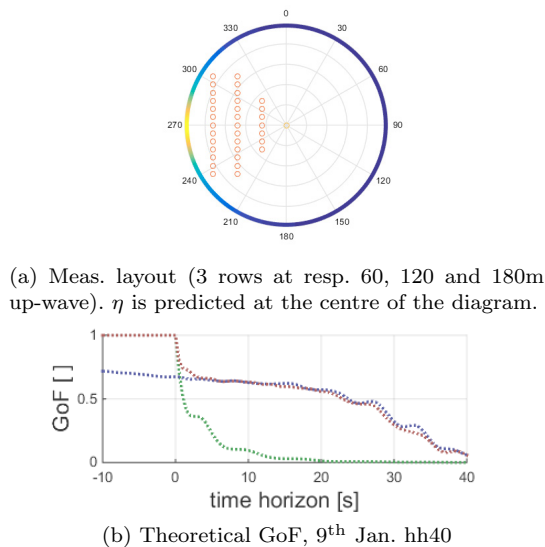

(b) Theoretical GoF, 9th Jan. hh40

Fig. 5. Theoretical GoF, in a hypothetical measurement layout. Green: TSC, blue: SDC, red: MC.

Finally, Fig. 5 shows what could theoretically be achieved with many more, far up-wave measurement locations, in a wave spectra from the 9th Jan. Of course, obtaining measurements at such a large number of points would require a different technology, such as an X-band radar, as did Belmont et al. (2014). Unsurprisingly, the forecasting horizon is greatly increased.

5. CONCLUSION

Overall, the ADCP measurement layout is not appropriate to yield accurate forecasts beyond a few seconds ahead. Schematically stated, larger distances between observation and prediction points would be necessary to increase the forecasting horizon, while a larger number of measurement locations would help capturing more of the wave directional spreading.

However, empirical SBP results using the ADCP layout are physically and statistically consistent. In particular, using more measurement locations improves the prediction accuracy; up-wave observations increase the forecasting horizon; and a broader frequency content negatively affects the prediction performance in all configurations. Finally, in spite of noise being present in the data, reasonably good agreement is found with the theoretically-optimal accuracy, the latter indicating the achievable performance with a given prediction configuration. Therefore, the SBP theoretical framework can provide useful guidelines with regards to the potential of specific prediction configurations, in given sea spectra.

ACKNOWLEDGEMENTS

REFERENCES

Abusedra, L. and Belmont, M. (2011). Prediction diagrams for deterministic sea wave prediction and the introduction of the data extension prediction method. *International Shipbuilding Progress*, 58(1), 59–81.

Belmont, M., Christmas, J., Dannenberg, J., Hilmer, T., Duncan, J., Duncan, J., and Ferrier, B. (2014). An examination of the feasibility of linear deterministic sea wave prediction in multidirectional seas using wave profiling radar: Theory, simulation, and sea trials. *Journal of Atmospheric and Oceanic Technology*, 31(7), 1601–1614.

de Boer, J.G. (1969). On the correlation functions in time and space of wind-generated ocean waves. Technical Report 160, SACLANT ASW Research Centre, La Spezia (Italy).

Eaton, M.L. (2007). Multivariate statistics: A vector space approach. *Lecture Notes-Monograph Series*, 53, i–512. URL http://www.jstor.org/stable/20461449.

Flanagan, J.D., Dias, F., Terray, E., Strong, B., Dudley, J., et al. (2016). Extreme water waves off the west coast of ireland: Analysis of ADCP measurements. In *Proceedings of the 26th International Ocean and Polar Engineering Conference*. International Society of Offshore and Polar Engineers.

Fusco, F. and Ringwood, J.V. (2010). Short-term wave forecasting for real-time control of wave energy converters. *IEEE Transactions on Sustainable Energy*, 1(2), 99–106.

Giron-Sierra, J.M. and Esteban, S. (2010). The problem of quiescent period prediction for ships: A review. volume 43, 307–312. Elsevier.

Hashimoto, N. (1997). Analysis of the directional wave spectrum from field data. *Advances in coastal and ocean engineering*, 3, 103–144.

Mérigaud, A. and Ringwood, J.V. (2018). Incorporating ocean wave spectrum information in short-term free-surface elevation forecasting. *IEEE Journal of Oceanic Engineering, Accepted*.

Naaijen, P. and Blondel-Couprie, E. (2012). Reconstruction and prediction of short-crested seas based on the application of a 3D-FFT on synthetic waves. Part 1: Reconstruction. In *Proceedings of the 31st International Conference on Ocean, Offshore and Arctic Engineering*, 43–53.

Naaijen, P., Trulsen, K., and Blondel-Couprie, E. (2014). Limits to the extent of the spatio-temporal domain for deterministic wave prediction. *International Shipbuilding Progress*, 61(3-4), 203–223.

Ochi, M.K. (2005). *Ocean Waves: The Stochastic Approach*. Cambridge University Press.